



Evaluation of IMERG Over CONUS Complex Terrain Using Environmental Variables

Y. Derin^{1,2}  and P.-E. Kirstetter^{1,2,3,4} 

¹Advanced Radar Research Center, University of Oklahoma, Norman, OK, USA, ²School of Meteorology, University of Oklahoma, Norman, OK, USA, ³School of Civil Engineering and Environmental Science, University of Oklahoma, Norman, OK, USA, ⁴NOAA/National Severe Storms Laboratory, Norman, OK, USA

Key Points:

- Conditional analysis of Integrated Multi-Satellite Retrievals for Global Precipitation Measurement (IMERG) using environmental parameters is conducted over mountainous terrain
- The hypothesis of “Does IMERG-Final quantification performance over complex terrain depend on orographically forced upward motion (w) and horizontal moisture flux convergence (Q) environmental parameters” proven to be correct
- Satellite-based precipitation product algorithms should incorporate environmental parameters to improve or adjust Level-2 or Level-3 estimates over complex terrain

Correspondence to:

Y. Derin,
yagmur.derin@ou.edu

Citation:

Derin, Y., & Kirstetter, P.-E. (2022). Evaluation of IMERG over CONUS complex terrain using environmental variables. *Geophysical Research Letters*, 49, e2022GL100186. <https://doi.org/10.1029/2022GL100186>

Received 24 JUN 2022
Accepted 20 SEP 2022

Author Contributions:

Conceptualization: Y. Derin
Funding acquisition: P.-E. Kirstetter
Methodology: Y. Derin, P.-E. Kirstetter
Project Administration: P.-E. Kirstetter
Software: Y. Derin
Supervision: P.-E. Kirstetter
Validation: Y. Derin
Visualization: Y. Derin, P.-E. Kirstetter
Writing – original draft: Y. Derin, P.-E. Kirstetter
Writing – review & editing: Y. Derin, P.-E. Kirstetter

Abstract Satellite-based precipitation products (SPPs) provide extensive spatial and temporal coverage globally but are challenged in complex terrain. This study aims at understanding uncertainties of SPP estimation due to topographically induced rainfall. Environmental and physical parameters, that is, orographically forced upward motion and horizontal moisture flux convergence, are considered to condition precipitation mechanisms for a detailed uncertainty analysis. The Global Precipitation Measurement (GPM) precipitation product Integrated Multi-Satellite Retrievals for GPM (IMERG) is compared at its native resolution against a high quality and accurate radar and rain gauge precipitation reference Ground Validation Multi-Radar Multi-Sensor (GV-MRMS). Conditional analysis of IMERG using environmental parameters is conducted over mountainous terrain. The highest GV-MRMS mean rainfall rate is found to be associated with positive high Q and moderate w values, confirming that vigorous moisture flux convergence is a strong condition for heavy rainfall. IMERG shows over- and underestimation for positive w and Q when GV-MRMS rainfall magnitudes between 0.8 and 13 mm h⁻¹.

Plain Language Summary Mechanisms by which topography affect precipitating clouds depend on many environmental and physical factors, so estimating precipitation over complex terrain is challenging. Ground-based measurement systems are sparse and cannot provide frequent and fine resolution coverage. Satellite-based precipitation products (SPPs) provide frequent and global but indirect precipitation estimation over mountainous terrain. This study aims at understanding uncertainties of the Integrated Multi-Satellite retrievals for Global Precipitation Measurement (IMERG) SPP against the high-quality Ground Validation Multi-Radar Multi-Sensor (GV-MRMS) precipitation product. Physical and environmental parameters (availability of moisture (Q) and lifting (w)) are used to focus the analysis on orographic precipitation. It is shown that IMERG detection and quantification performances over complex terrain highly depends on physical and environmental parameters. The highest GV-MRMS mean rainfall rate is found to be associated with positive high Q and moderate w values, confirming that vigorous moisture flux convergence is a strong condition for heavy rainfall. IMERG shows over- and underestimation for positive w and Q when GV-MRMS rainfall magnitudes between 0.8 and 13 mm h⁻¹.

1. Introduction

The influence of complex terrain on precipitation patterns causes some of the most pronounced climate gradients on Earth, conditions freshwater resources, and plays a fundamental role in triggering natural hazards like floods, landslides, and avalanches. Hence, the representation of the spatial and temporal distribution of precipitation over complex terrain is important. Unfortunately, this environment poses challenges to ground-based observation networks (Hou et al., 2014). Satellite-based precipitation products (SPPs) offer an alternative due to their ability to capture the space-time variability of rainfall with quasi-global coverage.

The great success of the Tropical Rainfall Measuring Mission (TRMM) and its successor Global Precipitation Measurement (GPM) mission accelerated the development of precipitation retrieval algorithms. For example, the Integrated Multi-satellitE Retrievals for GPM (IMERG) combines infrared (IR) radiances and passive microwave (PMW) precipitation retrievals to take advantage of the strengths of both IR and PMW and create global-scale precipitation estimates at high spatiotemporal resolution. However, SPPs are challenged over complex terrain in terms of detection and quantification of precipitation (Derin & Yilmaz, 2014; Derin et al., 2016; Derin, Anagnostou, et al., 2019; Derin, Nikolopoulos, & Anagnostou, 2019; Dinku et al., 2008, 2010; Hirpa et al., 2010). In general,

SPP estimation uncertainty can be related to the indirect nature of the measurement, the spatial heterogeneity of the precipitation fields, the sensors resolution and sensitivity, and the retrieval algorithms. Specific biases have been reported with orographic precipitation, such as the difficulties originating from the scattering-based PMW algorithms to identify “warm rain” that occurs without substantial quantities of upper-level ice particles. The resulting underestimation is more distinct over mountainous regions (Derin et al., 2018; Kubota et al., 2009; Yamamoto et al., 2017).

Research efforts have been made to improve the accuracy of SPP estimates over complex terrain. Kwon et al. (2008) showed that the TRMM Microwave Imager (TMI) retrieval performance depends on the topographically forced upslope motion, lower-level wind, and horizontal moisture flux. These factors were used to develop correction factors in the Korean Peninsula. The authors concluded that the correction using low-level moisture convergence combined with slope shows significant improvement regardless of rainfall intensity. Shige et al. (2013) built on the Kwon et al. (2008) study and use orographically forced upward motion and moisture flux convergence to improve GSMaP heavy rainfall estimates associated with shallow orographic rainfall systems.

In the light of this literature and validation studies conducted by Derin and Yilmaz (2014), Derin et al. (2016, 2018), Derin, Anagnostou, et al. (2019), and Anagnostou et al. (2017), it is established that precipitation mechanisms over complex terrain are multifactorial and depend on environmental and physical parameters. Yet much of the literature on SPP validation over complex terrain is conducted against point-based in-situ measurements. Derin, Anagnostou, et al. (2019) concluded that while in-situ observations are extremely important, they only provide limited rainfall spatial representativeness over complex terrain. The spatial-scale mismatch between SPP and gauges should be considered by using observations from remote sensors that better characterize the spatial variability of precipitation over complex terrain. In this study, the high-resolution, high-quality precipitation estimates from the Ground Validation Multi-Radar/Multi-Sensor (GV-MRMS; Kirstetter et al., 2012, 2018, 2020) is used as ground reference at the native resolution of IMERG (30 min and 0.1°). The evaluation is conducted over various complex terrain regions in CONUS to gather diverse and representative features and trends, that can be extrapolated to other regions of the world. Such transferability and representativeness are unprecedented in the literature. Moreover, the investigation of links between SPP errors and environmental and physical parameters is an important step toward mapping precipitation in complex terrain and provides useful information to algorithm developers and data users. Environmental and physical parameters used by Shige et al. (2013; orographically forced upward motion and horizontal moisture flux convergence) are used to condition the matchup data sets to refine the analysis of SPP performance. This study aims to answer the following question: Do atmospheric conditions and interaction with topographic features condition IMERG-Final quantification performance over complex terrain?

2. Study Region and Data Sets

Complex terrain classification is performed by following Daly et al. (1994). The ASTER global digital elevation model version 2 with 1 arc-second (~30 m) resolution is used to compute elevation gradients for CONUS. Gradients less than 2 m/grid are classified as flat and disregarded from the analysis, and the rest of the pixel grids are classified as complex terrain (Figure 1a). Because interactions between atmospheric fluxes and terrain are driving factors of precipitation generation and satellite performance, complex terrain regions are isolated to focus our analysis on the orographically induced precipitation processes.

The ground-based, radar-rain gauge quantitative precipitation estimation (QPE), GV-MRMS reference is generated at 0.1° spatial and 30-min temporal resolution (Derin et al., 2021, 2022; Kirstetter et al., 2012, 2018). Advanced data integration techniques are used to create 2D precipitation mosaic grids and QPE by blending radar and rain gauge data to provide a high-quality reference data set (Kirstetter et al., 2012, 2014, 2015). GV-MRMS also provides a radar quality index (RQI) to represent the level of uncertainty, that is used to select the best ground-radar estimates that can be otherwise degraded in complex terrain (e.g., Delrieu et al., 2009). A high quality and standardized reference are obtained by removing GV-MRMS estimates associated with RQI estimates lower than 100% across the study domain for SPP validation. In this study, GV-MRMS is used over a period of 12 months in 2015.

The IMERG algorithm intercalibrates, merges and interpolates all available microwave retrievals, microwave-calibrated IR satellite estimates, and rain gauge measurements in two ways: (a) PMW data are morphed

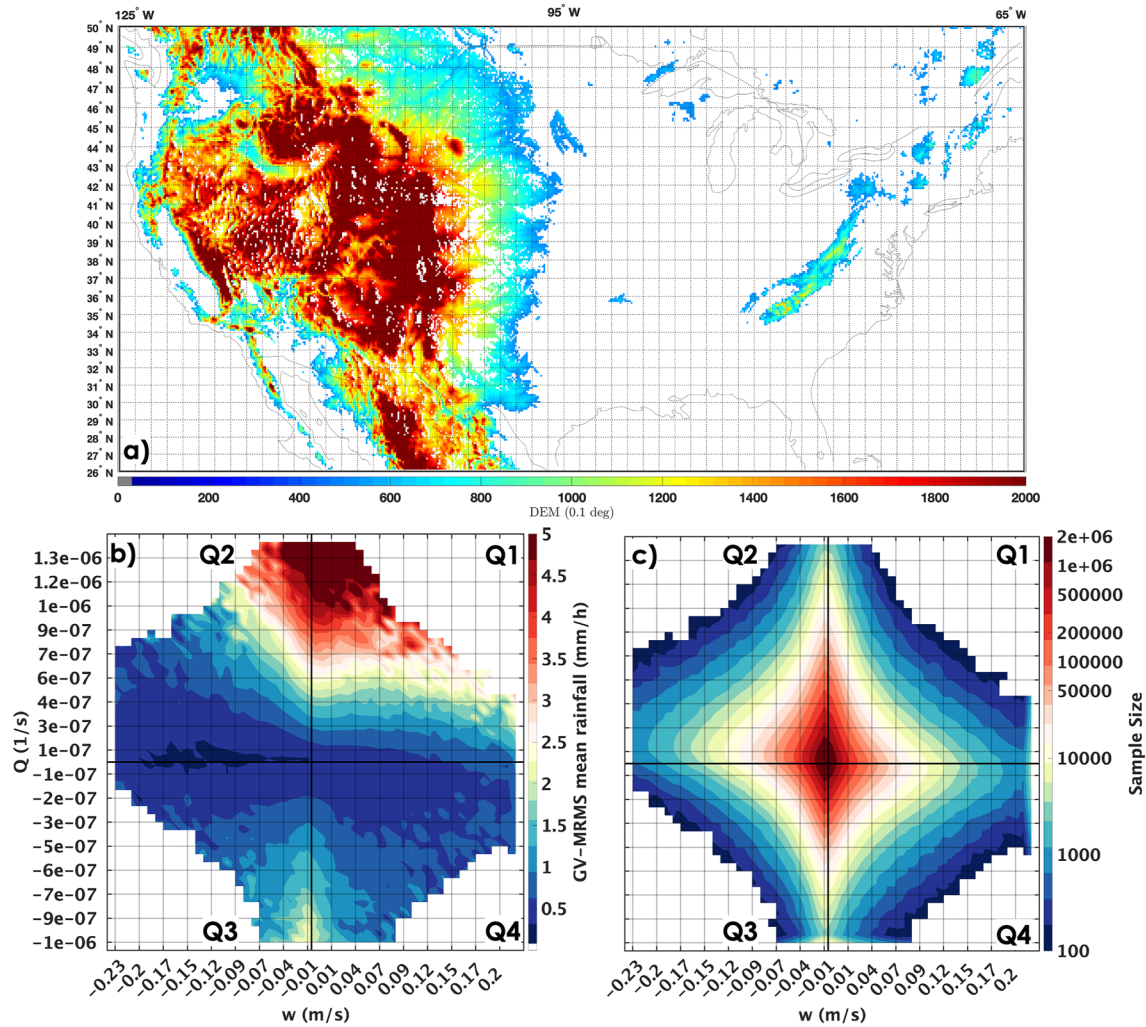


Figure 1. (a) The study region (CONUS) and the complex terrain regions. Bivariate histogram of GV-MRMS (b) mean rainfall magnitudes (mm/h) and (c) sample size as a function of w (m/s) and Q (1/s) environmental parameters.

using quasi Lagrangian time interpolation and estimated precipitation feature motion and (b) IR estimates are merged with PMW using a Kalman filter when PMW estimates are too sparse. IMERG is run twice in near-real time and once after the monthly gauge analysis is received for adjustment. IMERG Final “calibrated” fields are created by calculating ratios between the original monthly satellite-only and monthly gauge analysis. In this study, IMERG version 06B Final “calibrated” (IM-F) is evaluated at its native resolution of 30 min and 0.1° .

The Rapid Refresh (RAP) is the continental-scale NOAA hourly-updated assimilation/modeling system operational at NCEP at 13 km spatial resolution. RAP covers North America and is comprised primarily of a numerical forecast model and an analysis/assimilation system to initialize that model. The RAP uses the community-based Advanced Research version of the Weather Research and Forecasting Model (ARW) and the Gridpoint Statistical Interpolation analysis system (GSI) (Benjamin et al., 2016). To calculate the environmental parameters of orographically forced upward motion and horizontal moisture flux convergence, wind speed, relative humidity and temperature variables are obtained from RAP at the 13 km and hourly resolution.

3. Evaluation Method

The analysis is performed at the IM-F native resolution so that the comparison results remain free of undesirable impacts caused by statistical or dynamical resampling (Kirstetter et al., 2012, 2015). Only matched grids classified as complex terrain are used. GV-MRMS and IM-F rain/no rain threshold is set at 0.1 mm h^{-1} and

only matchup data sets with RQI of 100 (i.e., best quality) are used. Cells reporting snow are disregarded in this analysis. The comparison analysis is conditioned by environmental parameters driving orographic precipitation mechanisms.

Mechanisms by which mountains and hills affect precipitating clouds are complex and depend on many factors (Houze, 2012; Kirschbaum et al., 2018; Lin, 2007). Linear theory of orographic precipitation modeling characterizes orographic precipitation with two parameters since a good part of condensation is caused by forced ascent over fixed terrain (Barstad & Smith, 2005). The key components, as proposed by Barstad and Smith (2005), are the advection of vertically integrated condensed water with forced vertical motion. Orographic lifting of air mass depends on the direction of the incoming wind with respect to the orientation of the terrain barrier. Moisture transport depends on air parcel characteristics (i.e., temperature and relative humidity) and wind speed in the lower troposphere. Following Shige et al. (2013), orographic lifting and moisture availability are determined by orographically forced vertical motion (w , m/s) and horizontal moisture flux convergence (Q , s^{-1}) environmental variables. The vertical motion w can be estimated from the lower boundary condition flow over mountains (Lin, 2007):

$$w = \mathbf{V}_H \cdot \nabla h \quad (1)$$

where $h(x,y)$ is terrain height and \mathbf{V}_h is a surface horizontal wind vector. Surface horizontal wind values are calculated by using wind speeds from surface up to 700 hPa from RAP (13 km hourly resolution). Horizontal moisture flux convergence (Q , s^{-1}) can be calculated as (Banacos & Schultz, 2005):

$$Q = -\nabla \cdot (q\mathbf{V}_H) \quad (2)$$

where q is specific humidity (kg/kg).

Orographically forced vertical motion and horizontal moisture flux convergence can take on negative and positive values. In general, positive (negative) w magnitudes indicate an upward (downward) motion. Positive (negative) Q magnitudes indicate a moisture convergence (divergence) where vertically integrated moisture is increasing (decreasing) since moisture is concentrating (spreading out).

4. Results

Understanding the links between SPP uncertainty and horizontal moisture flux convergence and orographically forced vertical motion holds promises to diagnose SPP performance over complex terrain precipitation regimes and provide useful information to algorithm developers and data users. By relating these environmental parameters to heavy rainfall, Shige et al. (2013) categorized warm-rain processes that are enhanced by low-level orographic lifting of maritime air with thresholds applied on w ($w > 0.1 \text{ m s}^{-1}$) and Q ($Q > 0.5 \times 10^{-6} \text{ s}^{-1}$). This study follows a more systematic and quantitative approach by seamlessly considering the full spectrum of w and Q environmental parameters (including negative values associated with subsidence and flux divergence) that are associated with various precipitation mechanisms and magnitudes.

To improve our understanding of the relation between w , Q , and rainfall, and to be able to answer the question of “is there a relationship between environmental parameters and ground reference GV-MRMS,” Figure 1 displays a bivariate histogram of GV-MRMS rainfall (mm h^{-1}) as a function of w (m/s) and Q (s^{-1}). Each w and Q matched bin are colored by the average rainfall magnitude (in mm h^{-1}) of the corresponding GV-MRMS population (Figure 1b). Statistics are displayed when the sample size is greater than 100 (Figure 1c). Four quadrants are determined by the signs of w and Q , each of them representing different precipitation mechanisms over complex terrain. Quadrant (Q1) corresponds to positive w (upward motion) and Q (convergence); quadrant (Q2) corresponds to positive Q and negative w (downward motion); quadrant (Q3) corresponds to negative w and Q (divergence); quadrant (Q4) corresponds to positive w and negative Q . Figure 1 extends the depiction of precipitation variability outside conditions that are traditionally associated with warm orographic rain (Shige et al., 2013). Importantly, precipitation displays variability and transitions smoothly from one quadrant to another suggesting that thresholds applied on environmental conditions do not effectively isolate precipitation processes in complex terrain. The highest GV-MRMS mean rainfall rate are found to be associated with positive high Q values ($>7e^{-7} \text{ s}^{-1}$) and moderate w values in the range $(-0.09-0.12) \text{ (m s}^{-1}\text{)}$. It confirms that vigorous moisture flux convergence is a strong condition for heavy rainfall. The highest mean rainfall magnitudes observed by

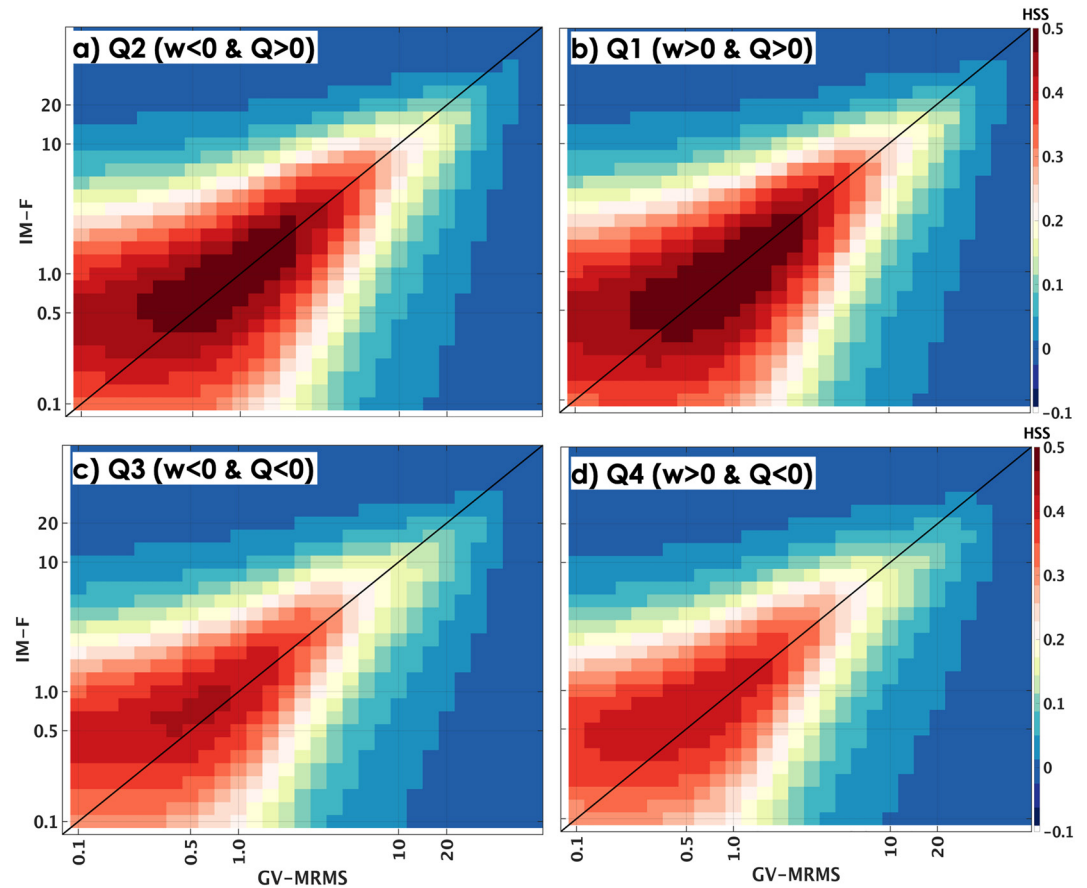


Figure 2. 2D HSS of IM-F conditioned by w and Q quadrants (a) Q2 ($w \leq 0$ m/s and $Q > 0$ 1/s), (b) Q1 ($w > 0$ m/s and $Q > 0$ 1/s), (c) Q3 ($w \leq 0$ m/s and $Q \leq 0$ 1/s), and (d) Q4 ($w > 0$ m/s and $Q \leq 0$ 1/s).

GV-MRMS over Q1 can be explained by shallow and deep convective rainfall mechanisms interacting with the topography, both of which producing heavy rainfall over short periods of time. Another precipitation mechanism that can be inferred for this quadrant is upward motion over heated terrain during daytime on both sides of the mountain that converges at the crest and form cumulus clouds. In Q2, GV-MRMS mean rainfall magnitudes decrease sharply toward higher negative w magnitudes. Negative w , positive Q , and light rainfall magnitudes in Q2 can be explained by lee side convergence due to diurnal variability (Kirshbaum et al., 2018). During daytime air moves into valleys and mountain gaps, converging in the lee side of the mountain (Hagen et al., 2011). During nighttime surface-based horizontal convergence focuses on lower altitudes surrounding orography. In Q3 the GV-MRMS average rainfall magnitudes decrease sharply when associated with low Q magnitudes (around 0 s^{-1}), meaning there is limited to no horizontal moisture flux for rainfall. The lowest GV-MRMS mean rainfall magnitudes are reported for negative w and Q values that are close to zero. 71.6% of the GV-MRMS mean rainfall magnitudes in Q3 are zero, and positive GV-MRMS average rainfall magnitudes are in the range (0–2) mm/h. The high end of rainfall rates in this quadrant are associated with higher magnitudes of negative Q . The relationship between GV-MRMS rainfall magnitudes (0.5–2) mm/h and moisture flux divergence and downward motion in this quadrant (Q3) will be investigated in future studies. From Figure 1b, GV-MRMS occurrence of zero rainfall in Q4 is on par with Q3 (70.4%). The highest GV-MRMS precipitation occurrence (36%) is reported in Q2 and followed by Q1 (27%). Meanwhile the lowest GV-MRMS occurrence is reported in Q4 (18%) and followed by Q3 (19%).

The detection capabilities of IM-F are analyzed with categorical skill scores. IM-F and GV-MRMS either do or do not detect rainfall and the performance of IM-F detection can be calculated with Heidke skill score (Heidke, 1926). The two-dimensional HSS approach (2D-HSS) is particularly useful for determining the optimum delineation of nonzero rain rates over challenging conditions (Derin et al., 2021; Petty & Li, 2013). Figure 2

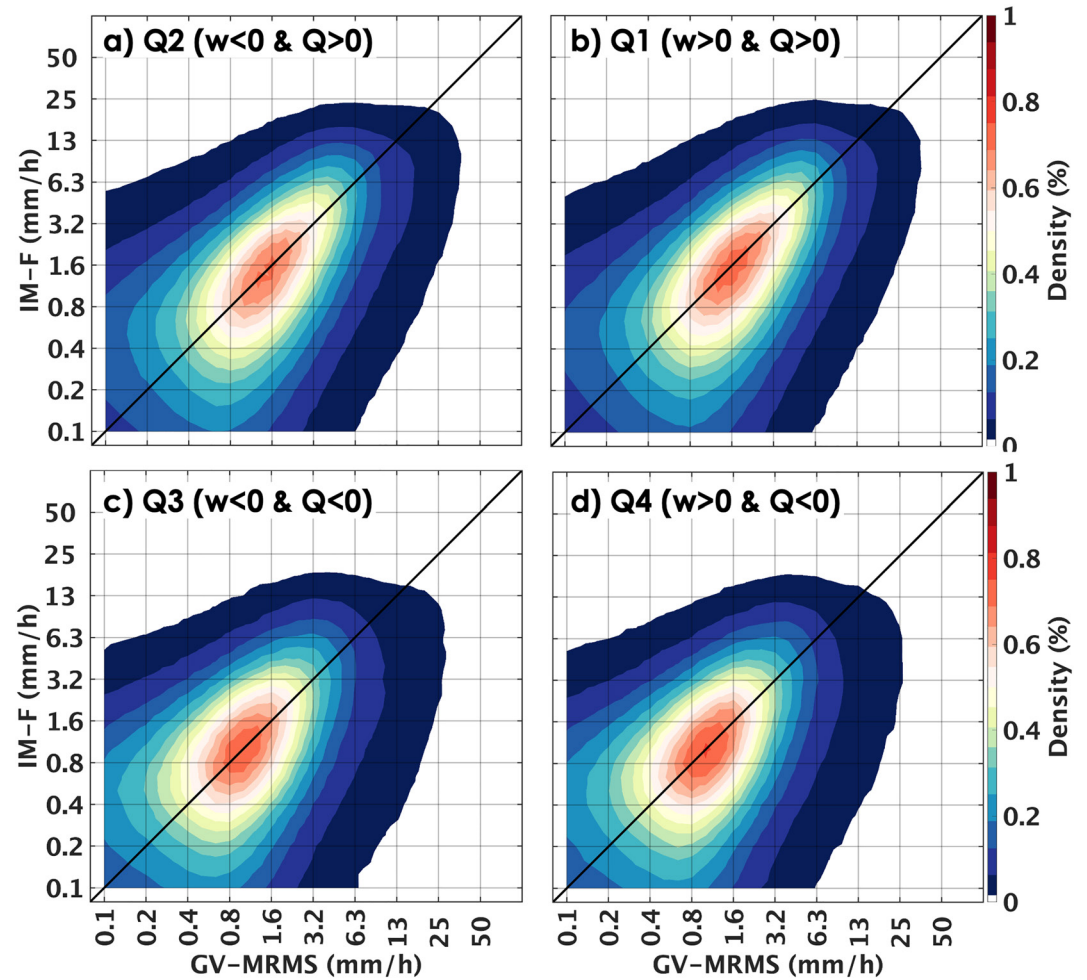


Figure 3. Density scatter plot of GV-MRS versus IM-F (mm/h) conditioned by w and Q quadrants (a) Q2 ($w \leq 0$ m/s and $Q > 0$ 1/s), (b) Q1 ($w > 0$ m/s and $Q > 0$ 1/s), (c) Q3 ($w \leq 0$ m/s and $Q \leq 0$ 1/s), and (d) Q4 ($w > 0$ m/s and $Q \leq 0$ 1/s).

quantify IM-F accuracy relative to that of random chance and determine the optimum precipitation delineation (see Derin et al., 2021 for more details). The colored map represents the HSS values for different thresholds applied both to GV-MRMS and IM-F for each quadrant (Q1, Q2, Q3, and Q4). The GV-MRMS (IM-F) rain/no-rain threshold values are indicated on the x -axis (y -axis). Overall, maximum HSS values are found in Q1 and Q2 corresponding to positive moisture flux convergence Q . It suggests that the magnitude of Q impacts IM-F detection performance more than vertical motions w . The highest HSS values over Q1 and Q2 (>0.4) are found in the precipitation rate range (0.3–5 mm/h), indicating that IM-F overall delineates these rainfall rates the best. HSS values decrease as we move to Q3 and Q4, highlighting challenges to delineate precipitation magnitudes in conditions of moisture flux divergence. Overall, IM-F rainfall detection and delineation of magnitude has significant dependence on different environmental conditions.

The quantification capabilities of IM-F can be analyzed with a density scatter plot. Next step investigates whether IM-F replicates such variability that we have seen with GV-MRMS in Figure 1. Extracting the full ranges of w and Q values extends the understanding of precipitation processes in complex terrain and provides a significant leverage in terms of understanding SPP uncertainty sources. Density scatter plots of GV-MRMS versus IM-F (mm h^{-1}) are plotted in Figure 3, conditioned by environmental parameters to provide additional insight on this relation. This plot provides limited insight to make inferences regarding IM-F overall performance compared to GV-MRMS as a function of w and Q environmental parameters. The performance of IM-F is visually similar across quadrants.

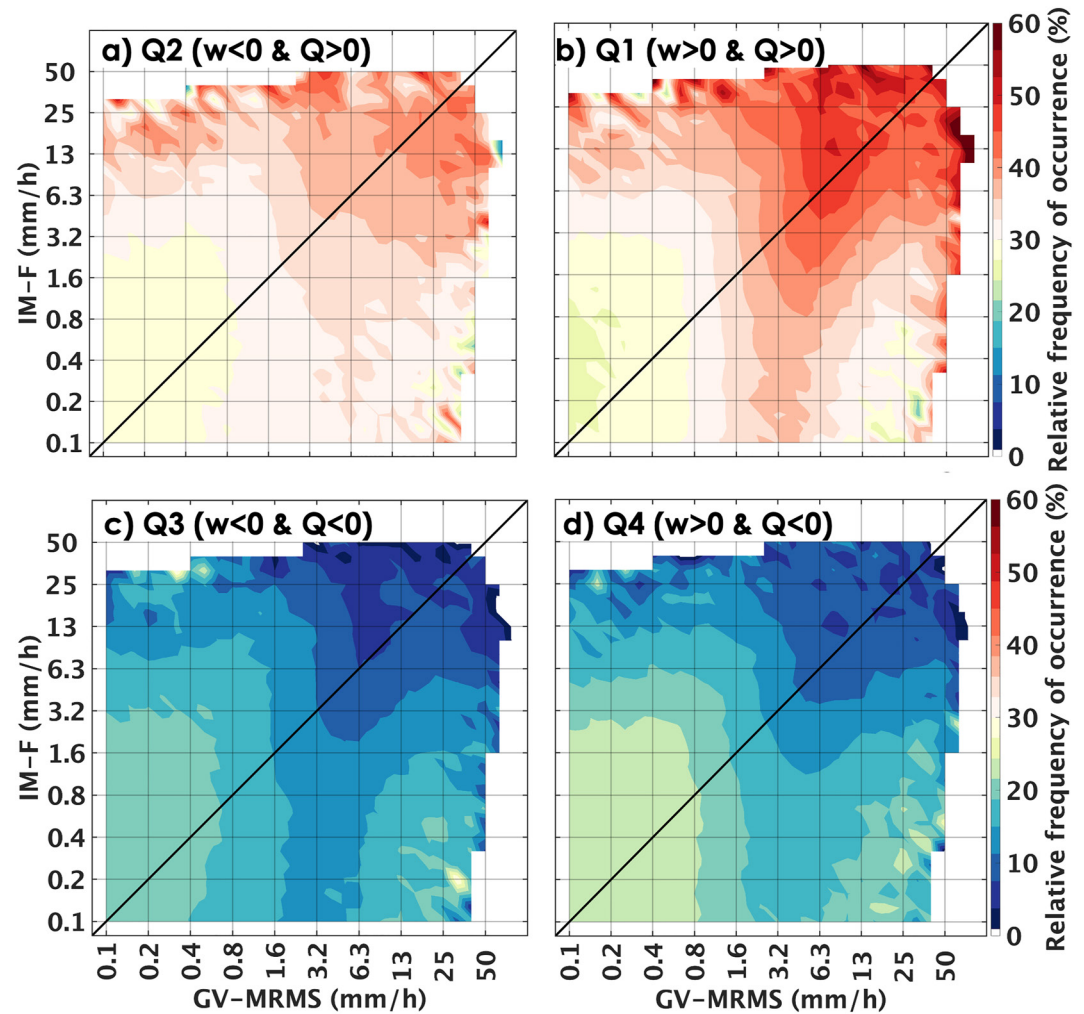


Figure 4. Relative frequency of occurrence of w (m/s) and Q (1/s) as functions of GV-MRMS and IM-F rainfall magnitudes (mm/h) conditioned by w and Q quadrants (a) Q2 ($w \leq 0$ m/s and $Q > 0$ 1/s), (b) Q1 ($w > 0$ m/s and $Q > 0$ 1/s), (c) Q3 ($w \leq 0$ m/s and $Q \leq 0$ 1/s), and (d) Q4 ($w > 0$ m/s and $Q \leq 0$ 1/s).

Density scatterplots (Figure 3) and bulk statistics (e.g., bias, correlation) show limited insight into the performance of IM-F (Kirstetter et al., 2020) and its sensitivity to the precipitation processes captured in different quadrants. More physical insight is provided in Figure 4 to understand how orographic enhancement mechanisms impact the performance of IM-F. For each pair of GV-MRMS, IM-F pair, Figure 4 shows the associated environmental conditions by displaying the relative frequency of occurrence for four quadrants. It indicates which environmental conditions and precipitation mechanisms are more often associated with a given GV-MRMS and IM-F precipitation rate pair and helps interpret the (dis)agreement between both products. The relative frequency of occurrence (%) of each of the four environmental conditions sums up to 100% for a given GV-MRMS and IM-F bin. If IM-F performance does not depend on the w and Q environmental parameters, then each panel in Figure 4 should be uniform. On the contrary, each panel highlights IM-F performance issues over complex terrain.

In general, higher GV-MRMS rainfall magnitudes (>3 mm h⁻¹) are associated with higher relative frequency of occurrence ($>40\%$) of w and Q parameters in Q1 and Q2 quadrants (positive Q magnitudes). On the other hand, lower GV-MRMS rainfall magnitudes (<1 mm h⁻¹) are associated with relatively higher relative frequency of occurrence (10%–30%) of w and Q parameters in Q3 and Q4 quadrants (negative Q magnitudes). It can be inferred that the magnitude of Q impacts precipitation more than the magnitude of w . In particular, Figure 4b (Q1, positive Q and w) shows that higher GV-MRMS rainfall magnitudes (>3 mm h⁻¹) are related to higher occurrence ($>40\%$) of positive Q and w (as also seen in Figure 1b). In this quadrant, IM-F shows significant over-

and underestimation for GV-MRMS rainfall magnitudes in the range (0.8–13) mm h⁻¹. This can be explained by shallow and deep convective rainfall mechanisms interacting with topography. Shallow orographic rainfall mechanisms generate low ice content compared to deep convection, hence the detection of shallow orographic rainfall mechanism by PMW is challenging. In Q1, IM-F probably underestimates shallow rainfall mechanisms and slightly overestimates deep convective rainfall mechanisms. Figure 4a (Q2) indicates that higher GV-MRMS rainfall magnitudes (>3 mm h⁻¹) are also related to higher occurrence (>30%) of positive Q and negative w . Note that IM-F performance in Q2 is slightly more uniform compared to Q1. A cluster with low GV-MRMS rainfall magnitudes ((0.1–0.5) mm h⁻¹) is overestimated by IM-F ((0.1–3.2) mm h⁻¹), with occurrence of approximately 30% $w < 0$ and $Q > 0$. The relative frequency of occurrence of w and Q in Q3 is highest (~15%) at lower GV-MRMS rainfall magnitudes (0–0.5 mm h⁻¹). Similar performance is observed in Q4. Mechanisms related to these rainfall magnitudes will be investigated further in a future study.

5. Conclusions

In this letter, IM-F quantification performance dependence on physical and environmental parameters over complex terrain is evaluated. This is performed through a novel and integrated approach using orographically forced vertical motion and horizontal moisture flux convergence to trace the performance dependence of IM-F on the environmental parameters. The analysis is conducted by conditional analysis of IM-F against ground reference GV-MRMS using environmental parameters.

The hypothesis “Does IM-F quantification performance over complex terrain depend on w and Q environmental parameters?” is confirmed. Understanding the links between IM-F quantification performance and environmental parameters is especially important for the development of multi-sensor precipitation products. It is suggested to incorporate these parameters in precipitation algorithm to improve orographic precipitation estimation.

Gebregiorgis and Hossain (2013) work showed the dominance of topography over climate features on SPP uncertainty, and they concluded that inclusion of climate information somewhat redundant since topography is also a governing factor for Koppen climate classification. While ingesting topography can help isolate SPP uncertainties over complex terrain, incorporating movement of atmosphere and moisture conditioned by topography gives us further insight into underlying sources of SPP uncertainty. Moreover, in this study it has been shown that bulk statistics and traditional graphical tools could mislead us into thinking that there is no “visible” trend or relationship. The performance dependence of IM-F on w and Q environmental parameters were observed by using relative frequency of occurrence (%) instead of density (%).

This initial study is not the complete story however it is clear that orographic enhancement mechanisms can be characterized by environmental parameters. Considering the full spectrum of w and Q environmental parameters display precipitation variability that transition smoothly from one quadrant to another. The highest GV-MRMS mean rainfall rate are found to be associated with positive Q values ($>7e-07$ 1/s) and moderate w values in the range (–0.09–0.12 m/s), which confirms that vigorous moisture flux convergence is a strong condition for heavy rainfall. This can be associated with shallow and deep convective mechanisms interacting with topography. Light rainfall is observed in Q2 that can be interpreted as lee side convergence due to diurnal variability. IM-F shows significant performance dependence (significant over- and underestimation) for GV-MRMS rainfall magnitudes in the range (0.8–13) mm/h in Q1. It can be related to the IM-F underestimating shallow rainfall mechanisms and slightly overestimating deep convective mechanisms. The main take-way point is that satellite precipitation algorithms should incorporate environmental parameters to improve or adjust Level-2 or Level-3 estimates over complex terrain.

This study is conducted over the whole CONUS complex terrain. Significant performance differences may exist across regions, seasons, and satellite estimates which will be investigated in a future study. As future directions of this study, characterization of orographic rainfall will be refined, and mechanisms related to Q3 and Q4 will be investigated in more detail.

Data Availability Statement

The GV-MRMS precipitation data are available at the NASA Global Hydrology Resource Center (GHRC) (<http://dx.doi.org/10.5067/GPMGV/MRMS/DATA101>). The IMERG precipitation products are available online (<https://arthurhouhttps.pps.eosdis.nasa.gov>).

Acknowledgments

The authors acknowledge the efforts made by the NASA science team for making IMERG precipitation data accessible. Support from the NASA Global Precipitation Measurement Ground Validation program under Grant NNX16AL23G and the Precipitation Measurement Missions program under Grant 80NSSC19K0681 is acknowledged. The authors thank two anonymous reviewers whose comments helped to improve the paper.

References

- Anagnostou, M. N., Kalogiros, J., Nikolopoulos, E., Derin, Y., Anagnostou, E. N., & Borga, M. (2017). Satellite rainfall error analysis with the use of high-resolution X-band dual-polarization radar observations over the Italian Alps, Perspectives on Atmospheric Sciences. *Springer Atmospheric Sciences*. https://doi.org/10.1007/978-3-319-35095-0_39
- Banacos, P. C., & Schultz, D. M. (2005). The use of moisture flux convergence in forecasting convective initiation: Historical and operational perspectives. *Forecasters' forum*, 20(3), 351–366. <https://doi.org/10.1175/waf858.1>
- Barstad, I., & Smith, R. B. (2005). Evaluation of an orographic precipitation model. *Journal of Hydrometeorology*, 6(1), 85–99. <https://doi.org/10.1175/jhm-404.1>
- Benjamin, S. G., Weygandt, S. S., Brown, J. M., Hu, M., Alexander, C. R., Smirnova, T. G., et al. (2016). A North American hourly assimilation and model forecast cycle: The rapid refresh. *Monthly Weather Review*, 144(4), 1669–1694. <https://doi.org/10.1175/mwr-d-15-0242.1>
- Daly, C., Neilson, R. P., & Phillips, D. L. (1994). A statistical-topographic model for mapping climatological precipitation over mountainous terrain. *Journal of Applied Meteorology and Climatology*, 33(2), 140–158. [https://doi.org/10.1175/1520-0450\(1994\)033<0140:astmfm>2.0.co;2](https://doi.org/10.1175/1520-0450(1994)033<0140:astmfm>2.0.co;2)
- Delrieu, G., Boudevillain, B., Nicol, J., Chapon, B., Kirstetter, P., Andrieu, H., & Faure, D. (2009). Bollène-2002 Experiment: Radar quantitative precipitation estimation in the Cévennes-Vivarais region, France. *Journal of Applied Meteorology and Climatology*, 48(7), 1422–1447. <https://doi.org/10.1175/2008jamc1987.1>
- Derin, Y., Anagnostou, E., Anagnostou, M. N., Kalogiros, J., Casella, D., Marra, A. C., et al. (2018). Passive microwave rainfall error analysis using high-resolution X-band Dual Polarization radar observations in complex terrain. *IEEE Transactions on Geoscience and Remote Sensing*, 56(5), 2565–2586. <https://doi.org/10.1109/tgrs.2017.2763622>
- Derin, Y., Anagnostou, E., Berne, A., Borga, M., Boudevillain, B., Buytaert, W., et al. (2016). Multiregional satellite precipitation products evaluation over complex terrain. *Journal of Hydrometeorology*, 17(6), 1817–1836. <https://doi.org/10.1175/jhm-d-15-0197.1>
- Derin, Y., Anagnostou, E., Berne, A., Borga, M., Boudevillain, B., Buytaert, W., et al. (2019). Evaluation of GPM-era global satellite-based precipitation products over multiple complex terrain regions. *Remote Sensing*, 15(24), 2936. <https://doi.org/10.3390/rs11242936>
- Derin, Y., Kirstetter, P.-E., Brauer, N., Gourley, J. J., & Wang, J. (2022). Evaluation of IMERG satellite precipitation over land-coast-ocean continuum. Part II: Quantification. *Journal of Hydrometeorology*.
- Derin, Y., Kirstetter, P.-E., & Gourley, J. J. (2021). Evaluation of IMERG satellite precipitation over land-coast-ocean continuum. Part I: Detection. *Journal of Hydrometeorology*, 22, 2843–2859.
- Derin, Y., Nikolopoulos, E., & Anagnostou, E. N. (2019). Estimating extreme precipitation using multiple satellite-based precipitation products. In V. Maggioni & C. Massari (Eds.), *Extreme hydroclimatic events and multivariate hazards in a changing environment* (pp. 163–190). Elsevier. <https://doi.org/10.1016/B978-0-12-814899-0.00007-9>
- Derin, Y., & Yilmaz, K. K. (2014). Evaluation of multiple satellite-based precipitation products over complex terrain. *Journal of Hydrometeorology*, 15(4), 1498–1516. <https://doi.org/10.1175/jhm-d-13-0191.1>
- Dinku, T., Chidzambwa, S., Ceccato, P., Connor, S. J., & Ropelewski, C. F. (2008). Validation of high-resolution satellite rainfall products over complex terrain. *International Journal of Remote Sensing*, 29(14), 4097–4110. <https://doi.org/10.1080/01431160701772526>
- Dinku, T., Ruiz, F., Connor, S. J., & Ceccato, P. (2010). Validation and intercomparison of satellite rainfall estimates over Columbia. *Journal of Applied Meteorology and Climatology*, 49(2), 1004–1014. <https://doi.org/10.1175/2009jamc2260.1>
- Gebregiorgis, A. S., & Hossain, F. (2013). Understanding the dependence of satellite rainfall uncertainty on topography and climate for hydrologic model simulation. *IEEE Transactions on Geoscience and Remote Sensing*, 51, 1–718. <https://doi.org/10.1109/tgrs.2012.2196282>
- Hagen, M., van Baelen, J., & Richard, E. (2011). Influence of the wind profile on the initiation of convection in mountainous terrain. *Quarterly Journal of the Royal Meteorological Society*, 137(S1), 224–235. <https://doi.org/10.1002/qj.784>
- Heidke, P. (1926). Berechnung der Erfolges und der Gute der Windstarkevorhersagen im Sturmwarnungsdienst (Calculation of the success and goodness of wind strength forecasts in the Storm Warning Service). *Geografiska Annaler*, 8(4), 301–349. <https://doi.org/10.1080/20014422.1926.11881138>
- Hirpa, F. A., Gebremichael, M., & Hopson, T. (2010). Evaluation of high-resolution satellite precipitation products over very complex terrain in Ethiopia. *Journal of Applied Meteorology and Climatology*, 49(5), 1044–1051. <https://doi.org/10.1175/2009jamc2298.1>
- Hou, A. Y., Kakar, R. K., Neeck, S., Azarbarzin, A. A., Kummerow, C. D., Kojima, M., et al. (2014). The global precipitation measurement mission. *Bulletin American Meteorology Social*, 95(5), 701–722. <https://doi.org/10.1175/bams-d-13-00164.1>
- Houze, R. A., Jr. (2012). Orographic effects on precipitating clouds. *Reviews of Geophysics*, 50(1), rg1001. <https://doi.org/10.1029/2011rg000365>
- Kirshbaun, D. J., Adler, B., Kalthoff, N., Barthlott, C., & Serafin, S. (2018). Moist orographic convection: Physical mechanisms and links to surface-exchange processes. *Atmosphere*, 9(80). <https://doi.org/10.3390/atmos9030080>
- Kirstetter, P.-E., Hong, Y., Gourley, J. J., Cao, Q., Schwaller, M., & Petersen, W. (2014). A research framework to bridge from the Global Precipitation Measurement mission core satellite to the constellation sensors using ground radar-based National Mosaic QPE. In *Remote sensing of the terrestrial water cycle, AGU geophysical monograph series*. John Wiley.
- Kirstetter, P.-E., Hong, Y., Gourley, J. J., Chen, S., Flamig, Z., Zhang, J., et al. (2012). Towards a framework for systematic error modeling of spaceborne precipitation radar with NOAA/NSSL ground radar-based national mosaic QPE. *Journal of Hydrometeorology*, 13(4), 1285–1300. <https://doi.org/10.1175/jhm-d-11-0139.1>
- Kirstetter, P.-E., Hong, Y., Gourley, J. J., Schwaller, M., Petersen, W., & Cao, Q. (2015). Impact of sub-pixel rainfall variability on spaceborne precipitation estimation: Evaluating the TRMM 2A25 product. *The Quarterly Journal of the Royal Meteorological Society*, 141(688), 953–966. <https://doi.org/10.1002/qj.2416>
- Kirstetter, P.-E., Karbalae, N., Hsu, K., & Hong, Y. (2018). Probabilistic precipitation rate estimates with space-based infrared sensors. *The Quarterly Journal of the Royal Meteorological Society*, 144(S1), 191–205. <https://doi.org/10.1002/qj.3243>

- Kirstetter, P.-E., Petersen, W., Kummerow, C. D., & Wolff, D. B. (2020). Integrated multi-satellite evaluation for the global precipitation measurement: Impact of precipitation types on spaceborne precipitation estimation, In *Satellite precipitation measurement*, Advances in global change Research (Vol. 69, pp. 583–608). Springer.
- Kubota, T., Shige, S., Aonashi, K., & Okamoto, K. (2009). Development of nonuniform beamfilling correction method in rainfall retrievals for passive microwave radiometers over ocean using TRMM observations. *Journal of the Meteorological Society of Japan*, 87A, 153–164. <https://doi.org/10.2151/jmsj.87a.153>
- Kwon, E.-H., Sohn, B.-J., Chang, D.-E., Ahn, M.-H., & Yang, S. (2008). Use of numerical forecasts for improving TMI rain retrievals over the mountainous area in Korea. *Journal of Applied Meteorology and Climatology*, 47(7), 1995–2007. <https://doi.org/10.1175/2007jamc1857.1>
- Lin, Y. L. (2007). *Mesoscale dynamics* (p. 630). Cambridge University Press.
- Petty, G. W., & Li, K. (2013). Improved passive microwave retrievals of rain rate over land and ocean. Part II: Validation and intercomparison. *Journal of Atmospheric and Oceanic Technology*, 30(11), 2509–2526. <https://doi.org/10.1175/JTECH-D-12-00184.1>
- Shige, S., Kida, S., Ashiwake, H., Kubota, T., & Aonashi, K. (2013). Improvement of TMI rain retrievals in mountainous areas. *Journal of Applied Meteorology and Climatology*, 52(1), 242–254. <https://doi.org/10.1175/jamc-d-12-074.1>
- Yamamoto, M. Y., Shige, S., Yu, C.-K., & Cheng, L.-W. (2017). Further improvement of the heavy orographic rainfall retrievals in the GSMaP algorithm for microwave radiometers. *Journal of Applied Meteorology and Climatology*, 56(9), 2607–2619. <https://doi.org/10.1175/jamc-d-16-0332.1>